Optics Letters

Optimal generation and isolation of attosecond pulses in an overdriven ionized medium

Xiangyu Tang,[1] Kan Wang,[1] Baochang Li,[1] Yanbo Chen,[1] C. D. Lin,[2] and Cheng Jin[1,*]

[1]Department of Applied Physics, Nanjing University of Science and Technology, Nanjing 210094, China
[2]J. R. Macdonald Laboratory, Department of Physics, Kansas State University, Manhattan, Kansas 66506, USA
*Corresponding author: cjin@njust.edu.cn

Received 24 August 2021; revised 19 September 2021; accepted 20 September 2021; posted 20 September 2021 (Doc. ID 441365); published 6 October 2021

We identify optimal conditions for the generation and isolation of attosecond pulses in an overdriven ionized medium. In a high-pressure and highly ionized gas, the spatiotemporal wavefront rotation of a driving laser can be optimized, leading to complete spatial separation of successive attosecond bursts in the far field. The resulting isolated attosecond pulses (IAPs) are much more divergent such that they are spatially separated from the driving laser in the far field. We show that the time delay of near-field harmonic emission along the radial distance determines the divergence of the attosecond burst in the far field. The generated IAPs are phase matched upon propagation in the second half of the gas medium. Validity of the generation scheme is tested at different carrier–envelope phases for a few-cycle laser pulse and by synthesizing the fundamental and its second harmonic field for a long-duration pulse.

https://doi.org/10.1364/OL.441365

High harmonic generation (HHG) resulting from the nonlinear interaction between an intense laser and gas medium has become a useful table-top light source that can provide coherent radiation covering the spectral region from extreme ultraviolet (XUV) to soft x rays [1,2]. One of the most important applications of HHG is to produce isolated attosecond pulses (IAPs), with which electron dynamics in atoms and molecules occurring at the attosecond time scale can be probed and controlled [3]. Since the first IAP reported experimentally in 2001 by spectrally filtering high harmonics in the cutoff region [4], several temporal gating techniques have been developed for the generation of IAPs with the idea of making only one HHG emission burst prominent. These include polarization gating, double optical gating, ionization gating, transient phase-matching gating, synthesis of multi-color laser pulses, and so on [5–8]. Another promising route to generate IAPs is the spatial–temporal gating technique known as attosecond lighthouse. By using a driving laser with spatiotemporal coupling, characterized as wavefront rotation, which can be introduced by a pair of misaligned gratings or prisms before focusing, the emitted attosecond pulses will propagate in different directions, and thus are separated in space in the far field, despite that they are generated as a pulse train in the near field [9–11]. This method has been extended to generate attosecond soft x rays in the water window driven by a long-wavelength, few-cycle, 1.85-μm laser [12]. It has also been applied to dynamically increase the angular separation of individual attosecond pulses in a highly ionizing medium [13].

Similar to the technique of attosecond lighthouse, wavefront rotation can take place when an intense laser beam propagates in a highly ionizing gas medium since the spatiotemporal chirp is induced by the presence of free electrons [14,15]; thus, the generated attosecond pulses are expected to be spatially separated in the far field without any additional optical elements along the path of the generating beam. This idea has been tested theoretically by Tosa *et al.* [16] and Kovács *et al.* [17] by focusing infrared or mid-infrared high-intensity lasers into a relatively low-pressure Ar gas jet. The wavefront rotation of the laser pulse was clearly demonstrated, but the attosecond pulses were not spatially resolved. Thus, only an attosecond pulse train (APT) can be obtained after spatial filtering. Furthermore, the generation conditions were not optimal, and the spatial separation of the driving laser and the high harmonic beam was not achieved. On the other hand, in the overdriven regime, the complicated spatiotemporal reshaping of laser pulses often occurs, which has been used to produce IAPs on the axis in the far field via spatial filtering [18,19], but the attosecond pulses emitted at different time intervals were not spatially separated in the far field. Therefore, even though spatiotemporal reshaping or wavefront rotation of a laser pulse in a highly ionized medium has been intensively studied, how to optimally generate IAPs is still not available.

In this Letter, we will identify the conditions under which IAPs can be spatially well separated in the far field. We will show the difference between the traditional attosecond lighthouse and the similar one induced by ionization. We will analyze the dynamic phase-matching conditions for the optimal generation of IAP. We will also demonstrate the robustness of our method by checking its dependence on carrier–envelope phase (CEP) and for a two-color driving laser.

In our simulations, a single-atom response is calculated from quantitative rescattering (QRS) theory [20]; the propagation of the fundamental laser and high harmonic fields in the gas medium is computed from coupled three-dimensional

Maxwell's wave equations with cylindric symmetry. For the driving laser, dispersion of neutral atoms and free electrons and the absorption due to ionization are taken into account [21], while the nonlinear polarization and the dispersion and absorption of the gas medium are included for the generated harmonic field. High harmonics in the far field are obtained through a Hankel transformation according to their distribution (intensity and phase) at the exit plane of the medium. We employ a Gaussian beam as an incident laser with central wavelength of 800 nm. A temporal pulse envelope is assumed as Gaussian; its duration is 13.3 fs (five optical cycles) at full width of half maximum (FWHM), and its CEP is chosen as zero. The laser beam waist at focus is 60 μm. A 1-mm-long Ne gas jet with uniform density distribution is placed at the focus. Peak intensity at focus is 10×10^{14} W/cm^2, which is beyond the over-barrier intensity (approximately 8.6×10^{14} W/cm^2 for Ne), resulting in an initial ionization level over 30% on axis according to the modified Ammosov–Delone–Krainov (ADK) model [22].

We first vary the gas pressure, and show the simulated spectral intensity of the driving laser and the temporal intensity of generated attosecond pulses versus divergence in the far field at the optimal pressure of 600 Torr in Figs. 1(a) and 1(b), respectively. Due to the cylindric symmetry, the two-dimensional beam profile is expressed in terms of one-dimensional divergence. This is essentially different from the lighthouse technique where the beam of each IAP does not have circular shape. The intensity of the driving laser is mostly distributed within 4 mrad (indicated by the white line), close to the half-angle divergence of the undisturbed Gaussian beam, which is 4.2 mrad, defined as $\theta_{\mathrm{div}} = \lambda_0/\pi w_0$ with laser wavelength λ_0 and beam waist w_0. For attosecond pulses synthesized by high harmonics from 70 to 110 eV (conversion efficiency is 1.2×10^{-5}) in Fig. 1(b), there is no IAP generated on axis; instead, pulses labeled as 1, 2, and 3 individually appear as a single harmonic emission burst. Their divergences are all larger than 4 mrad, and thus they can be spatially separated from the fundamental laser. Such separation

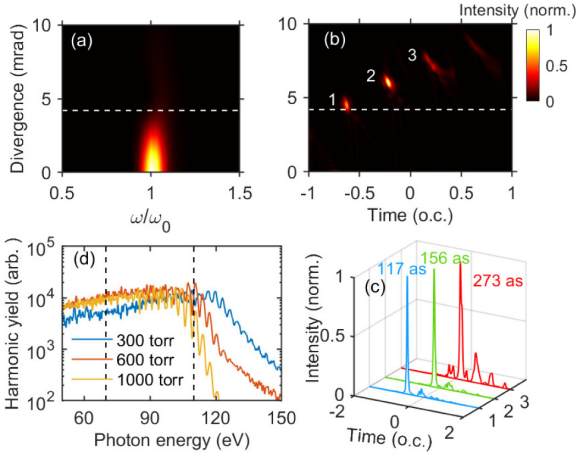

Fig. 1. Far-field intensity distribution (normalized) of (a) fundamental driving laser and (b) attosecond pulses. Note that pulses labeled as 1, 2, and 3 have donut-shaped beam profiles. (c) Isolated attosecond pulses in the far field via circularly spatial filtering, respectively performed within 4–5, 5.5–6.5, and 7–8 mrad. Attosecond pulses are synthesized by high harmonics in the spectral region of 70–110 eV. White dotted lines in (a) and (b) are used to mark the half-angle divergence of the initial Gaussian beam. ω_0 is the frequency of fundamental laser. (d) Total HHG spectra at the exit of the medium.

is very crucial if the driving laser has a high repetition rate, which has become a critical issue addressed recently [23,24]. This is quite different from most gating methods where the IAP is emitted on axis. When a circular spatial filter is applied, three IAPs with durations of 117, 156, and as 273 occurring at different time intervals can be obtained in Fig. 1(c). The calculated energy of most intense 156-as pulse is 2.4 nJ, which is very competitive for the generation of IAPs at ∼100 eV. Note that a large-sized spherical mirror is needed to refocus large-divergence IAPs. To mitigate this requirement, the divergence of IAPs can be reduced by using a more powerful driving laser under loosely focused geometry according to the macroscopic scaling rule given in Ref. [25], in which the product of gas pressure and medium length is a constant. As shown in Fig. 1(d), the total harmonic yields at 600 Torr are optimal since further increasing gas pressure only slightly reduces the cutoff energy and does not improve harmonic yields in the interested spectral region.

To understand the mechanism of IAP generation in the far field, we examine the spatiotemporal distribution of the driving laser and attosecond pulses at the exit plane of a gas medium. Figure 2(a) shows wavefront rotation of the laser pulse, which is caused by spatial and temporal variation of the refraction index due to the presence of the plasma effect. We have checked that a higher laser intensity is necessary if a shorter-duration pulse is applied to induce similar wavefront rotation. Since the ionization probability gradually increases with time, the wavefront depends not only on radial distance but also on time. This behavior is distinct from the technique of attosecond lighthouse in which wavefront rotation (or separation of successive field peaks) at a given spatial point is constant over the whole laser pulse. In our scheme, the laser pulse closer to the axis is more chirped, leading to harmonic emissions appearing at earlier times as shown in Fig. 2(b). For a given emission burst, the time delay between different radial positions r requires an optical path difference for compensation in the far field. Thus an attosecond pulse will be emitted off axis in the far field. We calculate its divergence by

$$\theta_f = c \cdot \frac{dt(r)}{dr}, \tag{1}$$

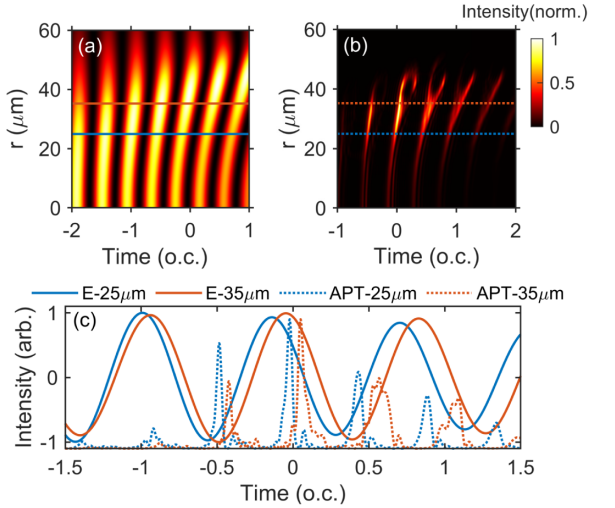

Fig. 2. Spatiotemporal intensity distribution of (a) fundamental driving laser and (b) attosecond pulses at the exit of gas medium. (c) Electric field (E) of driving laser and attosecond pulse train (APT) at $r = 25$ and 35 μm. Gas pressure is 600 Torr.

where c is the speed of light, and $t(r)$ is the spatially dependent emission time at the exit of the gas medium. We choose two radial distances at $r = 25$ and 35 μm in Figs. 2(a) and 2(b) (indicated by blue and brown lines) within which considerable harmonic yields can be seen, and we show the electric fields of the driving laser and intensity profiles of attosecond pulses versus time in Fig. 2(c). One can see that delays of emission time for attosecond bursts near −0.5 and 0 optical cycle (o.c.) are 0.15 and 0.21 fs, respectively. Thus, their divergences in the far field are calculated to be 4.5 and 6.3 mrad by using Eq. (1), which agrees very well with the direct numerical results (labeled as 1 and 2) in Fig. 1(b).

We next investigate the phase-matching mechanism of HHG during propagation in the gas medium. Figure 3(a) shows the electric fields of the driving laser and the corresponding ionization probabilities as a function of time at the entrance, middle, and exit of the gas medium. Due to the decreased ionization level, modification of the electric field from $z = 0$ to 0.5 mm is less significant than that from $z = -0.5$ to 0 mm. Thus a high harmonic field can be built up efficiently only in the second half of the gas medium, as shown in Fig. 3(b) for several selected harmonics. When the driving laser is reshaped during propagation, the harmonic coherence length $L_{\mathrm{coh}} = \pi/\Delta k$ can be calculated through the phase mismatch [26]

$$\Delta k_q \approx \frac{[(q-1)\,\omega_0 \Delta t - \alpha_i \Delta I]}{\Delta z}, \tag{2}$$

where q is the harmonic order, and ω_0 is the frequency of the driving laser. Δt and ΔI are the shift of peak electric field in time and intensity over a propagation distance Δz, respectively, which can be extracted from Fig. 3(a). α_i is the coefficient for calculating the phase accumulated over the electron trajectory in the laser field. We take the 81-eV harmonic as an example, and calculate its coherence length as in Table 1. The slowly varying electric fields between $z = 0$ and 0.5 mm could provide a favorable phase-matching condition for HHG. The largest coherence length occurs near −1 o.c. when the ionization level is close to the critical one (0.87% for Ne at 800 nm), so that the dispersion from a neutral atom and plasma is well balanced. The coherence length is then shortened significantly in the following optical cycles, which confines the effective harmonic generation within

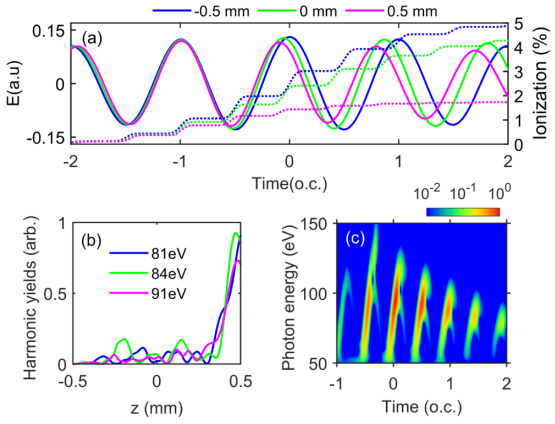

Fig. 3. (a) Electric field of driving laser (solid lines) and ionization level (dot lines) versus time at the entrance, middle, and exit of medium. (b) Evolution of harmonic field with propagation position z. (c) Time–frequency analysis of harmonics at the exit of medium. Radial distance is $r = 30$ μm.

Table 1. Coherence Length of 81-eV Harmonics at $r = 30$ μm Calculated by Eq. (2)[a]

Time (o.c.)	Δt (as)	ΔI (I_0)	L_{coh} (mm)
−1	8	−0.22	1.97
−0.5	−67	−0.60	0.38
0	−200	−1.05	0.12
0.5	−267	−1.35	0.09

[a] $\alpha_i \approx 1 \times 10^{-14}\,\mathrm{rad \cdot cm^2/W}$ for short-trajectory harmonics generated by the 800-nm laser. Δt and ΔI are read from Fig. 3(a) between $z = 0$ and 0.5 mm. $I_0 = 10^{14}\,\mathrm{W/cm^2}$.

a few optical cycles, as can be seen from the time–frequency harmonic emission in Fig. 3(c). This explains why only a few harmonic emission bursts have survived even though a five-cycle laser pulse is employed in Fig. 1(b).

We also check whether attosecond pulses can be spatially separated in the far field by using other gas pressures. For 300 Torr, the wavefront rotation in Fig. 4(a) is less severe than that at 600 Torr in Fig. 2(a), leading to near-field harmonic emission distributed from the axis to $r = 40$ μm and most bright emission bursts at −1 o.c. in Fig. 4(b). One can see that attosecond pulses with smaller divergences are not spatially resolved in Fig. 4(c). If gas pressure is increased to 1000 Torr, then wavefront rotation becomes very severe [see Fig. 4(d)]. Due to the excessive depletion of laser pulses near the axis, attosecond emission bursts are generated off axis near $r = 45$ μm, and the most intense one is emitted at a later time of 0.5 o.c. as shown in Fig. 4(e). According to Eq. (1), the divergence of attosecond pulses is expected to be larger. One can observe in Fig. 4(f) that attosecond pulses with larger divergence cannot be distinguished in space. Thus, the spatial filtering of far-field

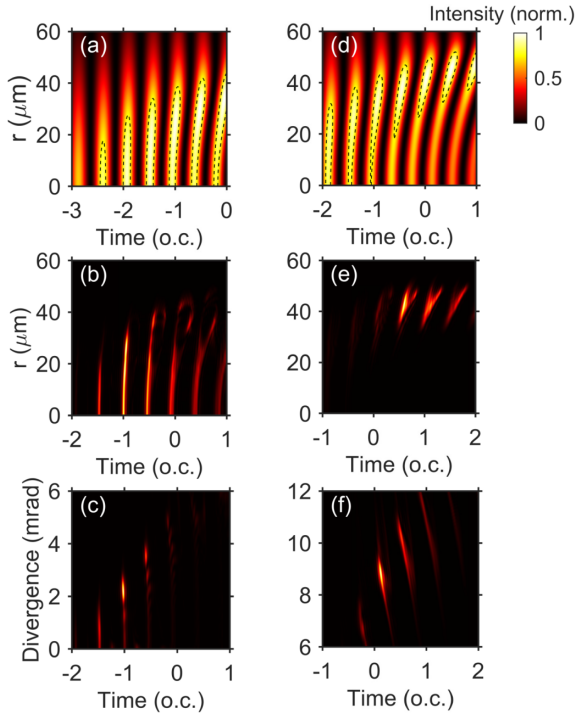

Fig. 4. Spatiotemporal intensity of driving laser at exit of medium, and attosecond pulses synthesized with high harmonics from 70 to 110 eV in near and far fields. The first and second columns are for 300 and 1000 Torr, respectively.

Table 2. Parameters of Single- and Two-Color Driving Lasers for Generation of Attosecond Pulses[a]

	λ (nm)	w_0 (μm)	I (I_0)	FWHM (fs)	CEP (π)
SC	800	60	10.0	26.7	0
TC	800	60	8.5	26.7	0
	400	30	0.5	26.7	0

[a]$I_0 = 10^{14}$ W/cm^2.

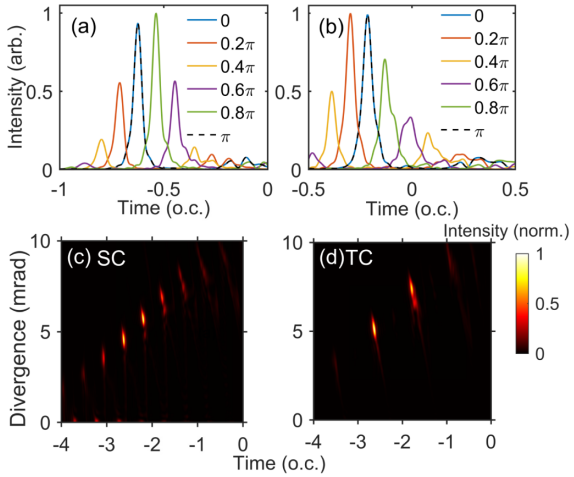

Fig. 5. Spatial filtered attosecond pulses from (a) 4–5 mrad and (b) 5.5–6.5 mrad in the far field at different CEPs driven by a five-cycle laser. Spatiotemporal intensity distribution of attosecond pulses in the far field driven by (c) 10-cycle single-color (SC) and (d) two-color (TC) laser pulses. o.c. is defined by the period of the 800-nm laser. Gas pressure is 600 Torr.

harmonics generated at these two pressures would always result in APTs.

We finally study the CEP effect on the generation of IAPs. As shown in Figs. 5(a) and 5(b), for two different circularly spatial filters, the IAP appears constantly in a wide range of CEPs, close to half π. CEP stabilization is still required for collecting IAPs. We also check the generation of attosecond pulses with long-duration single-color and two-color laser pulses. The laser parameters used in the simulations are listed in Table 2. In Fig. 5(c), more attosecond emission bursts show up with long-duration laser pulses, but spatial separation between successive bursts becomes worse compared to the few-cycle laser. To improve it, we propose to use a two-color laser pulse synthesized by an 800-nm laser and its second harmonic field so that the half-cycle periodicity of harmonic emission can be broken up. As shown in Fig. 5(d), the emission of an attosecond pulse takes place only once within one optical cycle of the 800-nm laser, and successive attosecond pulses can be clearly separated in space such that spatial filtering would result in IAPs.

In summary, we have demonstrated a robust and simple method for the optimal generation of IAPs from an ionized gas medium. Different from the traditional lighthouse technique, we have shown that successive attosecond pulses with donut-shaped beam profiles can be spatially separated. In addition, our method provides a route for the implementation of an efficient XUV pump/XUV probe scheme, in which two successive attosecond bursts can be spatially combined, and their relative time delay can be easily tuned by using independent refocusing optics.

Funding. National Natural Science Foundation of China (91950102, 11774175, 11834004); Chemical Sciences, Geosciences and Biosciences Division, Office of Basic Energy Sciences, Office of Science, Department of Energy (DE-FG02-86ER13491).

Disclosures. The authors declare no conflicts of interest.

Data Availability. Data underlying the results presented in this paper are not publicly available at this time but may be obtained from the authors upon reasonable request.

REFERENCES

1. F. Krausz and M. Ivanov, Rev. Mod. Phys. **81**, 163 (2009).
2. T. Popmintchev, M.-C. Chen, D. Popmintchev, P. Arpin, S. Brown, S. Ališauskas, G. Andriukaitis, T. Balciunas, O. D. Mücke, A. Pugzlys, A. Baltuška, B. Shim, S. E. Schrauth, A. Gaeta, C. Hernández-García, L. Plaja, A. Becker, A. Jaron-Becker, M. M. Murnane, and H. C. Kapteyn, Science **336**, 1287 (2012).
3. F. Calegari, G. Sansone, S. Stagira, C. Vozzi, and M. Nisoli, J. Phys. B **49**, 062001 (2016).
4. M. Hentschel, R. Kienberger, C. Spielmann, G. Reider, N. Milosevic, T. Brabec, P. Corkum, U. Heinzmann, M. Drescher, and F. Krausz, Nature **414**, 509 (2001).
5. J. Li, X. Ren, Y. Yin, K. Zhao, A. Chew, Y. Cheng, E. Cunningham, Y. Wang, S. Hu, Y. Wu, M. Chini, and Z. Chang, Nat. Commun. **8**, 186 (2017).
6. H. Mashiko, S. Gilbertson, C. Li, S. D. Khan, M. M. Shakya, E. Moon, and Z. Chang, Phys. Rev. Lett. **100**, 103906 (2008).
7. C. Hernández-García, T. Popmintchev, M. M. Murnane, H. C. Kapteyn, L. Plaja, A. Becker, and A. Jaron-Becker, Opt. Express **25**, 11855 (2017).
8. E. J. Takahashi, P. Lan, O. D. Mücke, Y. Nabekawa, and K. Midorikawa, Nat. Commun. **4**, 2691 (2013).
9. H. Vincenti and F. Quéré, Phys. Rev. Lett. **108**, 113904 (2012).
10. K. T. Kim, C. Zhang, T. Ruchon, J.-F. Hergott, T. Auguste, D. M. Villeneuve, P. B. Corkum, and F. Quéré, Nat. Photonics **7**, 651 (2013).
11. T. J. Hammond, G. G. Brown, K. T. Kim, D. M. Villeneuve, and P. B. Corkum, Nat. Photonics **10**, 171 (2016).
12. F. Silva, S. M. Teichmann, S. L. Cousin, M. Hemmer, and J. Biegert, Nat. Commun. **6**, 6611 (2015).
13. E. Balogh, C. Zhang, T. Ruchon, J.-F. Hergott, F. Quéré, P. Corkum, C. H. Nam, and K. T. Kim, Optica **4**, 48 (2017).
14. D. E. Rivas, B. Major, M. Weidman, W. Helml, G. Marcus, R. Kienberger, D. Charalambidis, P. Tzallas, E. Balogh, K. Kovács, V. Tosa, B. Bergues, K. Varjú, and L. Veisz, Optica **5**, 1283 (2018).
15. A. S. Johnson, D. R. Austin, D. A. Wood, C. Brahms, A. Gregory, K. B. Holzner, S. Jarosch, E. W. Larsen, S. Parker, C. S. Strüber, P. Ye, J. W. G. Tisch, and J. P. Marangos, Sci. Adv. **4**, eaar3761 (2018).
16. V. Tosa, J. S. Lee, H. T. Kim, and C. H. Nam, Phys. Rev. A **91**, 051801 (2015).
17. K. Kovács, M. Negro, C. Vozzi, S. Stagira, and V. Tosa, J. Opt. **19**, 104003 (2017).
18. M. B. Gaarde and K. J. Schafer, Opt. Lett. **31**, 3188 (2006).
19. C. Jin, A.-T. Le, C. A. Trallero-Herrero, and C. D. Lin, Phys. Rev. A **84**, 043411 (2011).
20. C. D. Lin, A.-T. Le, C. Jin, and H. Wei, J. Phys. B **51**, 104001 (2018).
21. M. B. Gaarde, J. L. Tate, and K. J. Schafer, J. Phys. B **41**, 132001 (2008).
22. X. M. Tong and C. D. Lin, J. Phys. B **38**, 2593 (2005).
23. C. Jin, X. Tang, B. Li, K. Wang, and C. D. Lin, Phys. Rev. Appl. **14**, 014057 (2020).
24. T. Gaumnitz, A. Jain, and H. J. Wörner, Opt. Lett. **43**, 4506 (2018).
25. C. M. Heyl, C. L. Arnold, A. Couairon, and A. L'Huillier, J. Phys. B **50**, 013001 (2017).
26. C. Jin, M.-C. Chen, H.-W. Sun, and C. D. Lin, Opt. Lett. **43**, 4433 (2018).